JACS JOURNAL OF THE AMERICAN CHEMICAL SOCIETY

Article

Cite This: J. Am. Chem. Soc. 2019, 141, 7376−7384

pubs.acs.org/JACS

Taming the Complexity of Donor−Acceptor Stenhouse Adducts: Infrared Motion Pictures of the Complete Switching Pathway

Habiburrahman Zulfikri,[†,+] Mark A. J. Koenis,[‡,+] Michael M. Lerch,[§] Mariangela Di Donato,[∥,⊥] Wiktor Szymański,[§,#] Claudia Filippi,[†] Ben L. Feringa,[*,§] and Wybren Jan Buma[*,‡,∇]

[†]MESA+ Institute for Nanotechnology, University of Twente, P.O. Box 217, 7500 AE Enschede, The Netherlands

[‡]Van 't Hoff Institute for Molecular Sciences, University of Amsterdam, Science Park 904, 1098 XH Amsterdam, The Netherlands

[§]Centre for Systems Chemistry, Stratingh Institute for Chemistry, University of Groningen, Nijenborgh 4, 9747 AG Groningen, The Netherlands

[∥]European Laboratory for Non Linear Spectroscopy (LENS), via N. Carrara 1, 50019 Sesto Fiorentino, Italy

[⊥]Istituto Nazionale di Ottica, Largo Fermi 6, 50125 Firenze, Italy

[#]Department of Radiology, University of Groningen, University Medical Center Groningen, Hanzeplein 1, 9713 GZ Groningen, The Netherlands

[∇]Radboud University, Institute for Molecules and Materials, FELIX Laboratory, Toernooiveld 7c, 6525 ED Nijmegen, The Netherlands

Supporting Information

ABSTRACT: Switches that can be actively steered by external stimuli along multiple pathways at the molecular level are the basis for next-generation responsive material systems. The operation of commonly employed molecular photoswitches revolves around one key structural coordinate. Photoswitches with functionalities that depend on and can be addressed along multiple coordinates would offer novel means to tailor and control their behavior and performance. The recently developed donor−acceptor Stenhouse adducts (DASAs) are versatile switches suitable for such applications. Their photochemistry is well understood, but is only responsible for part of their overall photoswitching mechanism. The remaining thermal switching pathways are to date unknown. Here, rapid-scan infrared absorption spectroscopy is used to obtain transient fingerprints of reactions occurring on the ground state potential energy surface after reaching structures generated through light absorption. The spectroscopic data are interpreted in terms of structural transformations using kinetic modeling and quantum chemical calculations. Through this combined experimental−theoretical approach, we are able to unravel the complexity of the multidimensional ground-state potential energy surface explored by the photoswitch and use this knowledge to predict, and subsequently confirm, how DASA switches can be guided along this potential energy surface. These results break new ground for developing user-geared DASA switches but also shed light on the development of novel photoswitches in general.

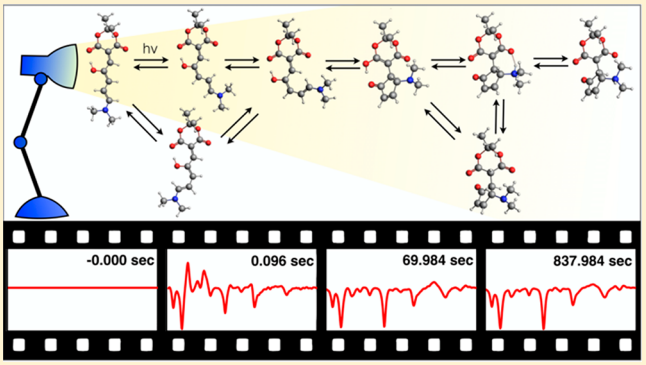

INTRODUCTION

Photochemical tools rely on light as external stimulus to manipulate chemical, biological, and materials systems with high spatiotemporal control and without contaminating the sample.[1,2] Molecular photoswitches[3] have been particularly successful in this respect as they can be switched reversibly between isomers[4] whose distinct properties can be harnessed in applications ranging from receptors[5] and molecular muscles[6] to machines[7−9] and "smart" materials.[10,11] More recently, they have been used for biological and medicinal applications, with photopharmacology attracting tremendous interest.[12−18] Switches such as azobenzenes,[19] stilbenes, hemithioindigos,[20] and diarylethenes[21] rely, for all practical purposes, on a simple transformation; that is, the key step for their functioning involves one reaction coordinate such as $E-Z$ isomerization or electrocyclization. Going beyond the possibilities offered by these "simple" systems requires photoswitches that undergo addressable transformations along multiple possible reaction pathways. Such switches open novel avenues for tailor-made, user-oriented chemical systems whose functionalities can be manipulated by directing the mechanistic pathway.

The recently introduced donor−acceptor Stenhouse adducts (DASA),[22−27] which have already found a wide range of

Received: January 10, 2019
Published: April 10, 2019

DOI: 10.1021/jacs.9b00341
J. Am. Chem. Soc. 2019, 141, 7376−7384

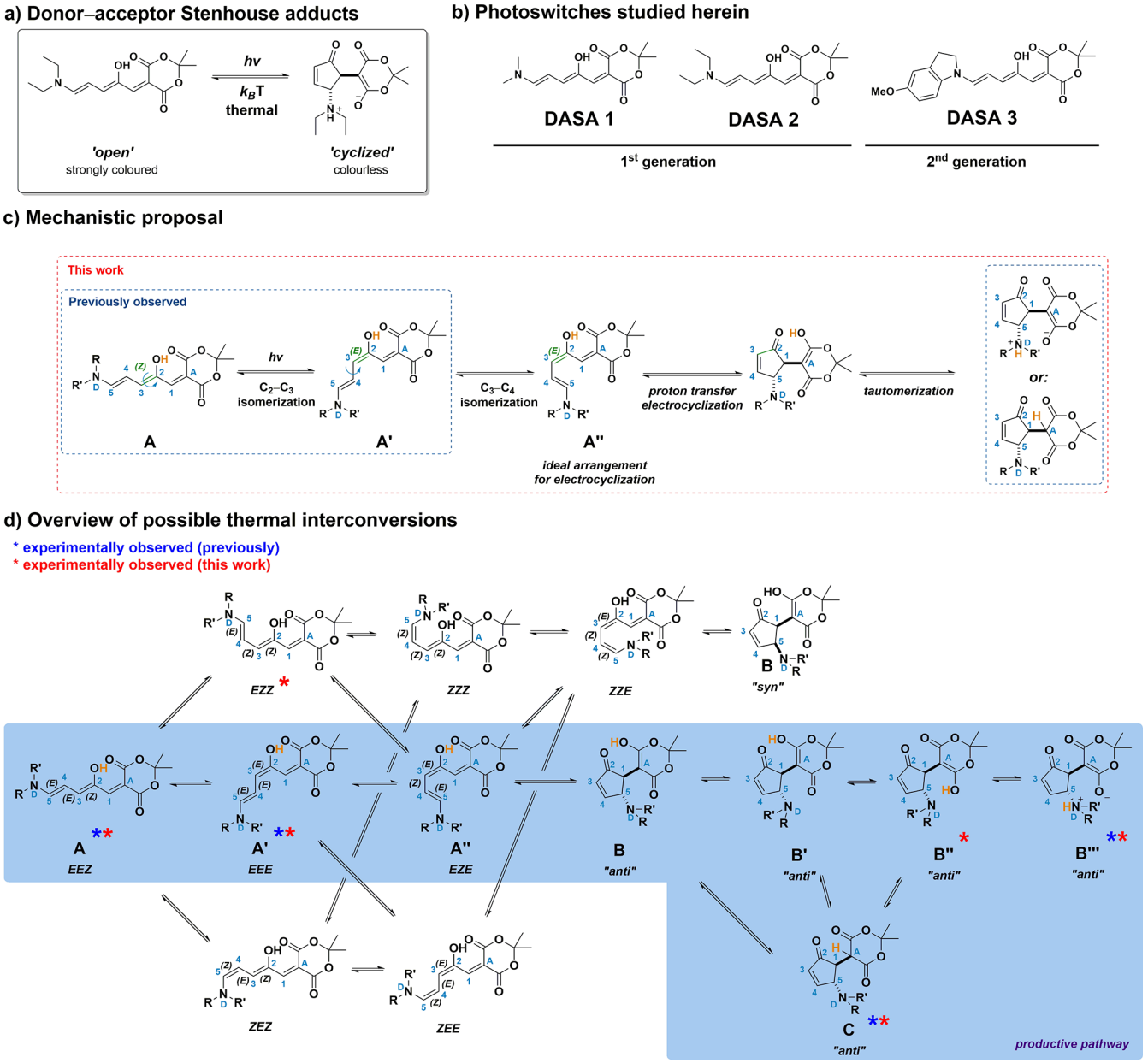

Figure 1. Donor–acceptor Stenhouse adducts: (a) overall photochemical transformation, (b) photoswitches studied in this work, (c) current mechanistic proposal for the photoswitching mechanism, and (d) all possible thermal interconversions.

applications,[27] feature in this respect favorable characteristics. The visible-light-triggered transformation starts from a strongly colored, linear triene ("open") that cyclizes into a colorless[28] cyclopentenone ("cyclized", Figure 1a), whose structure depends on the generation of DASAs used[24,25] (Figure 1b), and then thermally reverts to the original form. It has become clear (*vide infra*) that the functional use of DASAs along a productive photoswitching pathway depends on at least two key steps (see Figure 1c for mechanistic proposal):[23,29] a photo-induced Z–E isomerization within the triene and a thermal electrocyclization. Whereas the actinic step of the reaction has been previously investigated in detail,[29−32] insight into the thermal part of the pathway is as yet largely lacking. Here, using time-resolved infrared absorption spectroscopy and quantum chemical calculations, we show that competing photoswitching pathways are indeed far more complicated than one would have assumed *a priori*, and that rational control over it requires "turning knobs" that one normally would not consider.

Previous mechanistic studies of DASAs in solution have only focused on the initial photochemical step by means of ultrafast pump–probe spectroscopy and density functional theory (DFT) calculations, in combination with temperature-dependent steady-state UV/vis spectroscopy and photoaccumulation experiments at low temperature.[29−31,33] These investigations suggested Z–E isomerization happening on a picosecond time scale (from **A** to **A′** in Figure 1c).[30,31,33] The presence of a hydroxy group on the triene chain seems to favor the productive photochemical isomerization pathway around the C_2—C_3 bond,[31] but many different "nonproductive" isomers can potentially be obtained by thermal rotation or photochemical isomerization along the conjugated bridge[32] before and after photoactivation (Figure 1d). This increases the complexity of the switching process tremendously. In addition, gas-phase

DOI: 10.1021/jacs.9b00341
J. Am. Chem. Soc. 2019, 141, 7376−7384

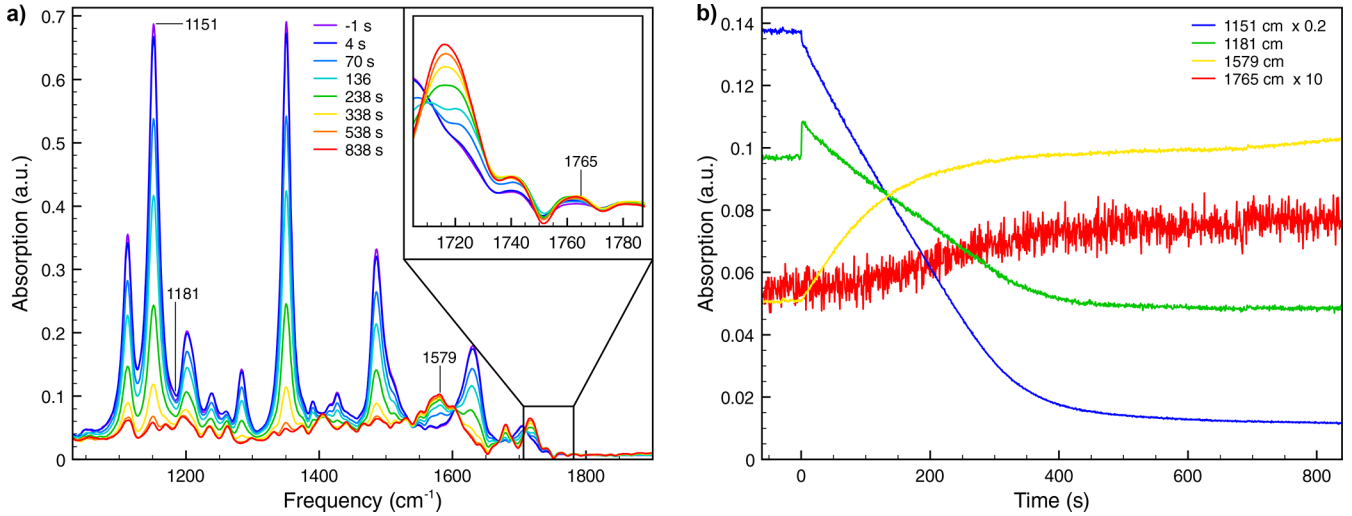

Figure 2. Rapid-scan FT-IR spectra of DASA **1**. (a) Snapshots of spectra before and after switching on the light (broadband white light, at $t = 0$) in the rapid-scan FT-IR experiment. (b) Time-dependent behavior of key bands during the rapid-scan FT-IR experiment. For the 1765 cm^{-1} trace, absorption is taken relative to the absorption at 1779 cm^{-1} in order to eliminate the change in absorbance due to other bands in the spectrum.

studies have suggested that the step following the initial photoisomerization could also be photochemical in nature, with **A**′ absorbing a second photon yielding **A**″.[32] This finding can be relevant for "real-life" applications of DASA switches for which usually continuous wave light sources are used as opposed to the pulsed laser sources employed in high-end spectroscopic studies.

In analogy to the Piancatelli rearrangement[34,35] and related (iso-)Nazarov-type[36] chemistry, it has been postulated that a productive mechanistic pathway involving a thermally allowed 4π-electrocyclization starting from **A**″ (Figure 1c) is followed by a proton transfer and tautomerization.[23,29] Although the primary photochemical step determines the immediate photoresponse, the thermal steps that occur on much longer time scales are far more important for understanding and controlling DASA-photoswitching. To characterize this thermal part of the switching mechanism, we employ a combination of rapid-scan IR absorption spectroscopy,[37] quantum chemical computations, and kinetic modeling. This approach offers the necessary time resolution (milliseconds to hours) and structural information to come for the first time to a complete picture of the thermal reaction pathways in DASAs in terms of calculated and observed intermediates, as well as their IR absorption spectra, energies, and possible ground-state interconversions. At the same time, it allows us to fill the gap between our ultrafast spectroscopy studies[30,31,33] and the photoswitching outcomes. We then show that the complicated reaction mechanisms are in fact governed by a few simple but sometimes counterintuitive principles that provide detailed design suggestions and guidelines for next-generation DASAs and that are applicable beyond the presently studied class of photochromes.

RESULTS AND DISCUSSION

Herein, we focused on three molecules (Figure 1b) representing both first- (**1** and **2**)[22,23] and second-generation (**3**)[24−26] DASA photochromes (SI sections 1.1, 2, and 7). To elucidate the molecular basis of the thermal interconversions and overall photoswitching mechanism, we identified the structures of the various isomers formed upon continuous wave illumination using rapid-scan FT-IR spectroscopy and kinetic modeling. Interpretation and assignment of the time-resolved spectra requires the comparison with computed IR spectra of all possible intermediates. We therefore optimized the structure of all ground-state minima and computed the corresponding vibrational spectra using DFT at the B3LYP[38,39]/maug-cc-pVDZ[40] level and an implicit SMD[41] solvent model. For the evaluation of the energy profile, we employed instead the M06-2X functional,[42] since B3LYP is known to describe incorrectly the ring-closure step[43] even though it produced better spectra for our systems (see SI Figure S5.33).

Photoinduced Thermal Reaction Pathways of DASA 1. Rapid-scan FT-IR spectra of DASA **1** in dichloromethane (DCM) are shown in Figure 2. Visual inspection of the time evolution makes immediately clear that most of the intense bands from the linear form **A** strongly decrease once light is switched on. As illumination progresses, new low-intensity bands appear as a result of cyclization, in particular in the carbonyl stretching region (1650−1750 cm^{-1}). Cyclization under continuous illumination is also observed by steady-state UV/vis spectroscopy (see SI section 3), manifesting itself in the disappearance of the intense absorption band in the visible spectral region, characteristic of the open form, and the increasing absorption in the UV region attributed to the closed form. The rapid-scan FT-IR experiments provide kinetic traces (Figure 2b) that allow us to distinguish three different phases in the reaction. Immediately after irradiation is started with broadband white light (see SI section 1.2), a quick response of the system occurs, producing a new equilibrium within the experimental time resolution of the experiment (96 ms). Subsequently, an exponential behavior is observed both in the decay of the starting compound and in the concurrent formation of a product. Importantly, time traces of bands in the carbonyl stretching region show different kinetics that suggests the delayed formation of another final product (see, for instance, the kinetic behavior of the red trace in Figure 2b as compared to the yellow trace).

To identify the minimum number of kinetic components needed to describe the time-dependent behavior of the spectra, we analyzed the rapid-scan FT-IR data using singular-value decomposition[44] (see SI section 1.7 for more details). Subsequently, we used a global analysis procedure[44] that fits the kinetic traces recorded at all frequencies simultaneously with

DOI: 10.1021/jacs.9b00341
J. Am. Chem. Soc. 2019, 141, 7376−7384

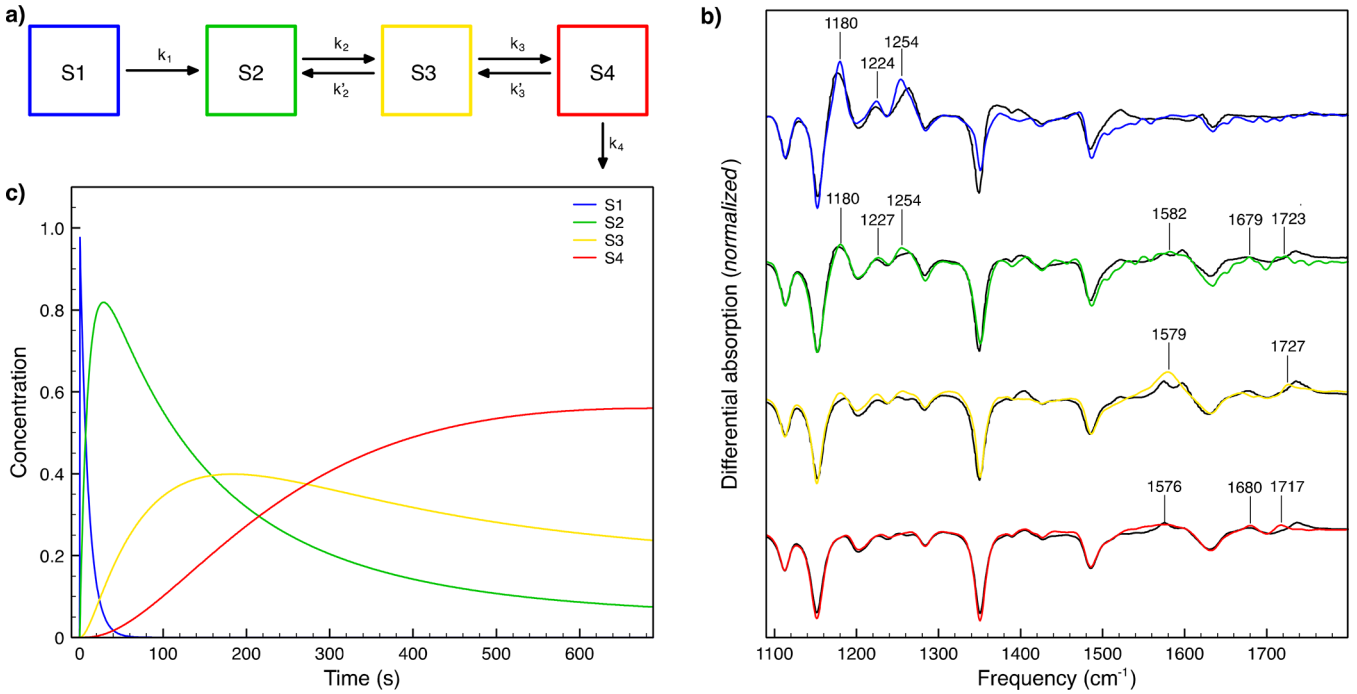

Figure 3. Kinetic scheme and modeling of the rapid-scan FT-IR measurement of DASA **1**. (a) Schematic representation of the kinetic model. (b) Resulting SADS (black) and their fits with computed spectra with SADS1 to SADS4 from top to bottom. The spectrum of the elongated form **A** has been subtracted before fitting the data, producing the differential signals shown in panel b. The four SADS have been fitted as follows (see Figure 1d for isomer notation): SADS1 a 37:63 mixture of **A′**/***EZZ***, SADS2 a 14:18:34:34 mixture of **A′**/***EZZ***/**B″**/**B‴**, SADS3 a 58:31:11 mixture of **B″**/**B‴**/**C** and SADS4 a 74:26 mixture of **B″**/**B‴**. (c) Concentration profile of the four SADS in time.

a combination of exponential decay functions. Global analysis requires the specification of a kinetic scheme, allowing to write the differential equations describing the change in the concentration of reactant and products and determine the associated kinetic constants. In view of the multitude of intermediate structures that may be formed during the reaction and the resulting complexity of the kinetic scheme describing their interconversion, the analysis was performed applying a simplified sequential reaction scheme shown in Figure 3a that nevertheless allows us to identify the time scale of formation of the main products.[44] The reaction scheme describes the time evolution of the system in terms of compartments (boxes S1−S4 in Figure 3a) representing the state of the system at a given time. The different compartments are connected by the kinetic constants determined from the fit of the kinetic traces. Apart from the kinetic constants, the analysis also determines the spectral component associated with each compartment. We loosely name these components "Species Associated Differential Spectra" (SADS) even though they do not reflect the differential spectra of pure intermediates (as in the case of a complete reaction scheme) but rather of mixtures due to the simplification here introduced. The four SADS resulting from the kinetic analysis with estimated lifetimes of t_1 = 10 s, t_2 = 88 s, t_3 = 201 s, and t_4 = 14 × 10^3 s are shown in Figure 3b. Assigning the positive/negative vibrational bands of each SADS to appearing/disappearing isomers during the course of the reaction requires knowledge of the energy profile of the productive lowest-energy pathway and the vibrational spectra of all intermediates along this pathway, which for clarity we split into three steps:

(1) From **A** to **A″** (Figure 4a). Our previous studies have shown that the primary photochemical step consists of photoisomerization around C_2—C_3 to form **A′**. This isomer can then thermally isomerize around C_3—C_4 to form **A″**, so that the molecule is spatially arranged for a thermally allowed, conrotatory 4π-electrocyclization step (Figure 1b).[30,33] Importantly, our calculations indicate that, besides the three open isomers (**A**, **A′**, and **A″**) put forward from the mechanistic proposal, one has to consider at least the isomer ***EZZ*** among the remaining five possible open isomers of Figure 1d (***EZZ***, ***ZZZ***, ***ZZE***, ***ZEZ***, and ***ZEE***), ***EZZ*** being the second most stable structure. ^{1}H NMR experiments confirm this finding as they show that the elongated triene form **A** is in thermal equilibrium with a minor amount of ***EZZ*** in solution at room temperature in the dark (see SI section 8).

(2) From **A″** to **B** (Figure 4b). For a successful ring-closure step, the electrocyclization of **A″** should be accompanied by a concomitant proton-transfer reaction (Figures 1c and 4) which breaks the extended conjugation and results in the formation of the colorless isomer **B**. An alternative electrocyclization without such an associated proton transfer is only possible in the absence of the intramolecular hydrogen bond. This pathway would involve a cyclized intermediate **I7** also involved in the pathway from **B** to **C** (see Figure 4c) that is high in energy (see SI Figure S6.4) and is thus unlikely to occur. Another possible but energetically disfavored electrocyclization pathway starting from the ***ZZE*** isomer (Figure 1d) would lead to a sterically encumbered *syn*-configuration in contrast to the energetically favored and experimentally observed[23,25,45] *anti*-configuration.

(3) From **B** onward (Figure 4c). To reach the lowest energy products, tautomerization of **B** to **B‴** or **C** needs to occur. While a solvent-assisted process was previously postulated,[33] it appears that a fast intramolecular proton-transfer pathway is possible without direct involvement of

DOI: 10.1021/jacs.9b00341
J. Am. Chem. Soc. 2019, 141, 7376−7384

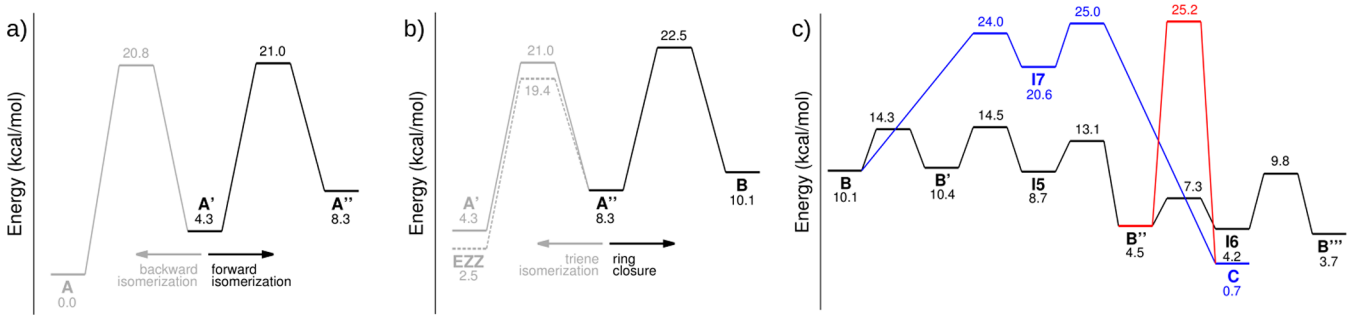

Figure 4. Possible isomers and calculated low-energy productive pathway. Energy profiles of DASA **1** in DCM for (a) backward (gray) and forward (black) isomerizations of the initial photoproduct **A′**, (b) triene isomerization (gray) and ring closure (black) of **A″**, and (c) the competing tautomerization pathways of **B** to **B‴** (black) and **C** (blue) and of **B″** to **C** (red).

solvent or another DASA molecule. Our calculations find that the system follows three consecutive steps to reach the zwitterionic final product **B‴**, a nitrogen inversion (**B′**), a rotation around C_1—C_A (**B″**), and a C_S—N_D bond rotation with a concomitant transfer of a proton to the nitrogen atom. We note that this path is energetically preferred among the many possible routes resulting from the combination of the above four processes, also when the possible ring-flip of the Meldrum's acid moiety is considered (see SI Figures S6.5–S6.7). The enol–keto tautomerization pathway from either **B** or **B′** to **C** (which is the primary cyclized product of DASA **3** as observed by ^{1}H NMR in CD_3CN and DMSO-d_6[25] and in crystal structures[24,25]) proceeds with a proton transfer mediated by the oxygen of the cyclopentenone ring, without any need for a catalyst, external acid, or base. Alternatively, the amine group on the cyclopentenone ring can facilitate the tautomerization from **B″** to **C** without any intermediates.

After identifying the lowest-energy pathway connecting the open and closed forms, the SADS obtained from the kinetic analysis of the experimental time-resolved IR spectra have been interpreted using the calculated IR spectra of the species reported in Figure 4. To this end, we fitted the SADS with combinations of the calculated spectra (reported in SI section S5.1.4) using an in-house developed genetic algorithm (see SI section S1.8).

Surprisingly, the first SADS **S1** (Figure 3b), which describes the species formed within the time resolution of the rapid-scan measurement (96 ms), shows a large contribution of ***EZZ***, which was not observed in our previous femtosecond time-resolved infrared (fs-TRIR) experiments that explored time delays up until the nanosecond time scale.[46] In particular, the two positive bands at 1224 and 1254 cm^{-1} observed in **S1** are missing in the fs-TRIR spectrum, which was previously assigned exclusively in terms of the formation of **A′** (SI Figure S5.20). Although the presence of a large amount of ***EZZ*** fits well with the energy of this isomer in comparison with **A′** and **A″**, the mechanism by which it is generated is not immediately clear, as the aforementioned TRIR experiments exclude photochemical generation from **A**. One possible explanation could be that a second photon absorption takes place, as recently put forward by Bieske and co-workers.[32] However, rapid-scan FT-IR experiments in which a band-pass filter (HQ510/80m-2p, Chroma) was used to inhibit absorption of a second photon by either **A′** or **A″**, which are both red-shifted with respect to **A**, show that this does not occur, since under these conditions ***EZZ*** is still formed with the same temporal behavior as without filter (see SI Figures S5.5 and S5.6). We therefore conclude that ***EZZ*** is generated along a thermal reaction path from **A′** (obtained photochemically within the time resolution of the experiment) to **A″** and then back to ***EZZ***. Considering the inherent uncertainties in calculated energy barriers, this path is energetically very well possible and in line with the observed time scales.

The second component (**S2** in Figure 3b) is formed on a 10 s time scale. Importantly, the IR spectra of closed isomers, in particular **B″** and **B‴**, needed to be included for an adequate fit. Notably, we observed bands at 1582 and 1723 cm^{-1} that are distinctive signatures of **B‴**, while the band at 1679 cm^{-1} can only be explained by **B″** (see SI Figure S5.17). The presence of the latter isomer is further supported by the observation of bands associated with its N–H bending and stretching modes at 1579 and 2200 cm^{-1} (see SI Figures S5.7and S5.17), which are significantly broadened and shifted as a result of the internal hydrogen bond in **B″**. We therefore conclude that after the "instantaneous" photoinduced transformation of **A** into other open isomers, ring closure can occur on a time scale of 10 s. In terms of Eyring's equation, this implies a Gibbs activation energy of 18.5 kcal/mol, which is in excellent agreement with the calculated Gibbs energy difference between **A′** and the transition state connecting **A″** to **B** (18.2 kcal/mol). Once the molecule has overcome this barrier, there is a downward energy path from **B** via **B′** that populates **B″** and **B‴**. The fact that **S2** shows contributions of **A′** and ***EZZ*** is due to the continuous generation of these isomers.

Subsequently, formation of **S3** occurs with a time constant of about 90 s (Figure 3b). What distinguishes this component from **S2** is the presence of the most stable closed isomer **C**, which is evidenced by the appearance of three characteristic carbonyl stretching bands in the spectrum (highlighted in Figure 2a), and the absence of open isomers. The fact that the formation of **C** occurs on a much longer time scale and that a delayed ingrowth is observed (Figure 2b, red trace) implies that tautomerization toward **C** starts from the closed **B**-type forms and is associated with a higher energy barrier. These conclusions are in good agreement with our calculations (Figure 4c), which show that after isomer **B** is formed, the tautomerization path with the lowest barrier is the one leading to **B‴** via **B″**. However, once these two isomers have been populated, a thermal reaction from **B″** to **C** is possible, albeit with a higher Gibbs activation energy, which explains its slower rate of formation.

The presence of a further component **S4** (Figure 3b) showing the presence of only **B″** and **B‴** and not of **C** may in first instance seem puzzling. Important to notice is that, in the sequential kinetic scheme adopted in Figure 3c, a particular SADS reports the changes that occur in the concentrations of the pertaining

DOI: 10.1021/jacs.9b00341
J. Am. Chem. Soc. 2019, 141, 7376–7384

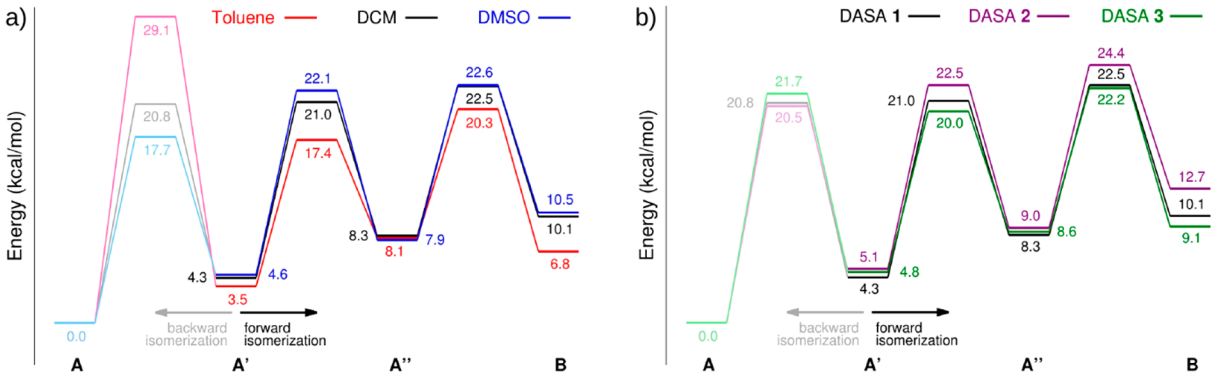

Figure 5. Role of solvent and substituent in the ring-closure reaction. Energy profiles for backward (lighter color) and forward (darker color) isomerization pathways of isomer **A′** of (a) DASA **1** in toluene (red), DCM (black) and DMSO (blue) and (b) all studied DASAs (**1** in black, **2** in purple, and **3** in green) in DCM.

components with respect to the previous SADS. This implies that in going from **S3** to **S4** the contribution of **B″** and **B‴** is affected to a major extent, while the contribution of **C** is much less affected. In our experiments on DASA **1**, dissolved in DCM, we have observed that precipitation occurs (see SI Figure S5.1). Such a precipitation does not occur when DASA **1** is dissolved in dimethyl sulfoxide (DMSO). Moreover, analyses of the rapid-scan FT-IR data on DASA **1** in DMSO do not show a fourth component (*vide infra*). The major difference between the two solvents is that in DMSO the zwitterionic **B‴** isomer is the end product and is very well soluble, while in DCM the solubility of **B‴** is considerably lower. We therefore conclude that the presence of **S4** for DASA **1** in DCM is due to the precipitation of **B‴**. This is in line with the observation that the concentration of **C** hardly changes in going from **S3** to **S4** and that the dominant changes occur in **B″** and **B‴**, with **B″** being influenced because it is on the pathway from **C** to **B‴** and has a nearly equal energy as **B‴** (Figure 4c). Such conclusion is also in agreement with the time scale on which **S4** decays (14×10^3 s), which, in turn, is in line with the Gibbs energy difference between **C** and the highest transition state leading to **B‴** (24.5 kcal/mol, Figure 4c).

The detailed studies presented above for DASA **1** in DCM have led to a series of remarkable and unexpected findings, highlighting the importance of thermal reaction pathways in determining both the rate and the efficiency of DASA photoswitching. The isomer ***EZZ*** is clearly observed and plays a key role in the early phase of photoswitching. Moreover, the cyclization occurs on a 10 s time scale consistent with the computed thermal barriers to produce **B**, which rapidly isomerizes to **B′** and then to **B″** and **B‴**. Subsequently, on a longer time scale, the most stable isomer **C** is formed.

Tailoring DASA's Reaction Pathways. Our experiments and calculations on DASA **1** show that the photoswitching process, although operationally simple, is in reality a picture of complex interconversions among different open and closed isomers where different tunable "knobs" allow controlling the overall photoswitching behavior. The experimental insights gained on the contribution of thermal interconversions and the developed theoretical model enable us to account for previously observed differences in the kinetic behaviors of DASA, which could depend on solvents or on the nature of donor or acceptor groups. Rationally addressing the key steps of the reaction by tuning the stability of selected isomers or the energetic barriers that regulate their thermal conversions, allows us to deliberately steer efficacies, rates, and switching characteristics of DASAs, as will be shown in the following.

The reaction scheme depicted in Figure 4 predicts the stability of the transition states from **A′** to **A″** and back from **A′** to **A** to be a key means to control the reaction rate of DASAs conversion. With the electrocyclization being the rate-limiting step, this is counterintuitive. A simple way to tune the energy of transition states is to change the solvent. Indeed, calculations with DMSO as a solvent show that the transition state between **A′** and **A** is 3.4 kcal/mol lower than in DCM, while the transition state to **A″** is only slightly higher by 0.8 kcal/mol (Figure 5a). In agreement with these findings, we observe experimentally that in DMSO full conversion of DASA **1** does not occur even after 3 h of irradiation, while in DCM ring closure proceeds on the order of minutes. As the energy profile of the ring-closure step (**A″** to **B**) is practically the same in both solvents, the lower conversion rate can only be attributed to a quicker thermal back conversion from **A′** to **A** in addition to a possible influence of band overlap.[33] This is confirmed by rapid-scan FT-IR studies (sections S5.1.2 and S5.1.3) that show almost no evidence for the presence of **A′** on the millisecond time scale, in agreement with the calculations that predict the half-life of **A′** to drop to around 1 ms in DMSO.

Further support for the importance of the stabilities of the transition states from **A′** to **A″** and back to **A** is found by analyzing the photoswitching behavior of DASA **1** in toluene. Here, faster photoswitching than in DCM is observed, in line with the lower/higher barrier for the forward/backward thermal conversion of **A′** predicted by the calculations (Figure 5a). The relative energy of the barriers can simply be explained by analyzing the bonding characteristics in different solvents (SI Figure S6.8). As the solvent polarity increases, the zwitterionic resonance contribution gains more importance, and consequently, the bond order of C_2—C_3/C_3—C_4 decreases/increases, thereby favoring/hindering isomerization around these bonds. The same consideration applies to the stability of the transition state from **A″** to ***EZZ***: higher barriers are found in toluene preventing the formation of the nonproductive ***EZZ*** isomer (SI Figure S6.9). From all these findings, we thus conclude that to increase the forward switching rate both the transition state from **A″** to ***EZZ*** and that from **A′** to **A** should be destabilized as much as possible to minimize counterproductive backward reactions.

Being able to control the composition of photostationary states is highly desirable when dealing with photoswitches. Although the use of different substituents on a particular donor is an obvious means to target this issue for DASAs, as exemplified by the recent studies of Beves and co-workers,[45] it is quite unexpected that replacing the methyl groups in DASA **1**

DOI: 10.1021/jacs.9b00341
J. Am. Chem. Soc. 2019, 141, 7376−7384

by ethyl groups in DASA **2** leads to major changes in photoswitching behavior (for DASA **2** cyclization is much reduced, see SI section 3.2). Rapid scan FT-IR spectra of DASA **2** in DCM recorded directly after switching on the light are very similar to those of DASA **1** in the same solvent, indicating comparable early steps (SI Figure S5.20). Hence, differences in the overall photoswitching behavior should be a result of differences in energies at later stages. Our calculations find indeed that the ring-closure step (from **A″** to **B**) is responsible for the slower photobleaching in DASA **2** (Figure 5b), which can be related to the steric hindrance arising from the bulkier ethyl groups. This seems to hold for different solvents as well, since switching experiments in toluene (SI section S3.2) found that DASA **2** converts more slowly to the cyclized product than DASA **1** (see also the energy profile in SI Figure S6.18). Fine-tuning of steric interactions thus appears to be more instrumental in regulating DASA's switching pathways than expected. Thus, substitutions at the triene unit could very well be another useful means to obtain further control over DASA's photoswitching behavior, and this is indeed one of the directions we are presently exploring.

By now, several generations of DASAs have been developed that aim for further control by modifying the electronic properties of the donor and acceptor groups. Our studies on DASA **3** (see SI sections S5.3 and S6.4), an example of a second-generation DASA, demonstrate how the present investigations allow for rationalizing in much more detail how specific donors influence the switching behavior. Importantly, already the actinic step is dramatically influenced by a change in donor: excitation of isomer **A** of DASA **3** leads to the formation of both **A′** and ***EZZ*** in equal amounts, in contrast to the first-generation DASAs (compound **1** and **2**) where only **A′** is formed. Using a combination of ^{1}H NMR, ultrafast TR-IR, rapid-scan FT-IR experimental data and DFT calculations, we find that most likely a forked photochemical reaction pathway is responsible for this behavior (see Figure 6). ^{1}H NMR *in situ*-irradiation experiments

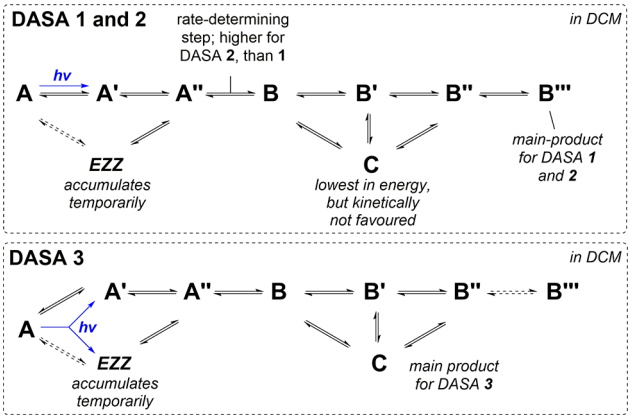

Figure 6. Overview of photoswitching behavior of DASA **1**−**3** in DCM.

support this finding as both **A′** and ***EZZ*** accumulate rapidly (see SI section 9). The fact that upon irradiation ***EZZ*** is easily formed in DASA **3** can help explain previously observed differences[33] in the behavior of first- and second-generation DASAs. In these ultrafast time-resolved IR spectroscopic studies, it was observed that for nanosecond delays the spectra of compound **2** showed solvent-dependent changes, while for compound **3** the same spectral features were observed for all solvents. This observation can now be understood: in first-generation DASAs, the interconversion between **A′** and ***EZZ*** is a thermal process whose barrier depends on the employed solvents whereas for second-generation DASAs the formation of ***EZZ*** is photo-induced and solvent independent. We expect the photochemical forked pathway of DASA **3** to be a direct result of a further weakening of the double bonds in the triene due to the aromaticity of the indoline group. Since ***EZZ*** is not part of the productive switching pathway, the efficacy of such switches is in principle reduced.

Our rapid-scan FT-IR studies on DASA **3** (SI section S5.3) further show that in DCM only **C** is formed as suggested previously,[24,25] in line with the prediction that this isomer is considerably more stable than the **B** forms (SI Table S6.14). However, what in first instance would not have been expected but is in excellent agreement with the calculated higher energy barrier between **B** and **C** is that several forms of **B** can be observed as intermediates, except **B‴**, which is markedly destabilized, most likely due to the decreased basicity of the donor. The destabilization of the zwitterionic **B‴** helps to prevent the formation of precipitated products for DASA **3** as compared to DASA **1** in chlorinated solvents.

Overall, thermal interconversions between isomers thus prove to be essential for DASA photoswitching (Figure 6). First generation DASAs **1** and **2** predominantly produce **A′** through light absorption, but the unproductive ***EZZ*** isomer can be accumulated via a solvent dependent thermal interconversion through **A″**. In contrast, DASA **3** exhibits a forked photochemical reaction to produce both **A′** and ***EZZ***. With a complete understanding of the thermal reaction steps involving the electrocyclization, proton transfer, and tautomerizations leading to the cyclized forms, we now can start acting on the molecular structure to deliberately steer the outcome and kinetics of DASA photoswitching and to produce application-tailored switches.

CONCLUSIONS

Photoswitching of DASAs **1**−**3** has been studied using rapid-scan FT-IR to elucidate the structural transformations at work after photoexcitation and their time scales. Key to the interpretation of these data has been a complete mapping of the reaction pathway with all possible intermediates and transitions states. This has led to a detailed understanding of the switching pathways, energies, and barriers governing the thermal equilibrium. Overall, a picture has emerged in which thermal interconversions play a crucial role in the photoswitching of DASAs.

While the primary photochemical step provides an initial means to kick-start the process, the rate-limiting thermal steps govern the overall behavior of these switches. Unexpectedly, thermal interconversions not only play a central role in the electrocyclization and proton-transfer/tautomerization steps, but also in the arrangement of the DASA structure for electrocyclization as has been outlined above for the role played by the ***EZZ*** isomer. The photochemical step gives access to high-energy open intermediates, and it is the control over the lifetime of these intermediates that allows one to steer the reaction toward a targeted outcome. Once electrocyclization takes place, rapid interconversion of the primary closed species **B** to other **B**- and **C**-type closed forms is possible, with a product distribution that can be directed according to the specific application at hand. The herein presented results have clarified for the first time where modifications need to take place to achieve a particular photoswitching behavior, enabling operators to steer DASA's photoswitching outcome along multiple switching pathways.

DOI: 10.1021/jacs.9b00341
J. Am. Chem. Soc. 2019, 141, 7376−7384

DASAs have entered the molecular nanotechnology field only recently but have evolved tremendously over the past few years. The beauty of these switches relies on their complex reaction pathway that allows tuning of their photoswitching and overall behavior with interventions in structure and environment. The "IR motion pictures" recorded in the present work together with elaborate quantum chemical calculations that supply crucial "subtitles" have provided the insight necessary to do so in a rational manner, at any point, and at a level that was not possible before.

EXPERIMENTAL SECTION

Rapid-Scan FT-IR. The samples were prepared in a dark room. Subsequently 10−15 min rapid-scan FT-IR measurements have been performed using a Nicolet iS50 FT-IR spectrometer at a resolution of 8 cm^{-1} and a sampling rate of 10.4 s^{-1}. For samples that did not fully convert within 15 min a 3−3.5 h kinetics measurement was performed with the same spectrometer using a resolution of 4 cm^{-1} and a sampling rate of 1 s^{-1}. After 30−60 s a ThorLabs OSL2 high-intensity fiber light source was switched on at maximum power at <3 cm in front of the sample. More detailed information about the experiments is given in the Supporting Information (SI section 1).

ASSOCIATED CONTENT

Supporting Information

The Supporting Information is available free of charge on the ACS Publications website at DOI: 10.1021/jacs.9b00341.

All experimental procedures and characterization of compounds, steady-state UV/vis spectra and ultrafast visible and mid-IR spectra, kinetic analysis, measured and calculated vibrational absorption spectra, and full computational details (PDF)

AUTHOR INFORMATION

Corresponding Authors

*b.l.feringa@rug.nl
*w.j.buma@uva.nl

ORCID

Michael M. Lerch: 0000-0003-1765-0301
Mariangela Di Donato: 0000-0002-6596-7031
Wiktor Szymański: 0000-0002-9754-9248
Claudia Filippi: 0000-0002-2425-6735
Ben L. Feringa: 0000-0003-0588-8435
Wybren Jan Buma: 0000-0002-1265-8016

Author Contributions

[+]H.Z. and M.A.J.K. contributed equally to this work.

Notes

The authors declare no competing financial interest.

ACKNOWLEDGMENTS

This work was supported financially by The Netherlands Organization for Scientific Research (NWO-CW, Top grant to B.L.F., VIDI Grant No. 723.014.001 for W.S., NWO Chemical Innovations Project No. 731.014.209 to W.J.B.), the European Research Council (ERC; Advanced Investigator Grant, No. 694345 to B.L.F.) and the Ministry of Education, Culture and Science (Gravitation program, No. 024.001.035). The computational work was carried out on the Dutch national supercomputer Cartesius with the support of the SURF Cooperative. Furthermore, the authors acknowledge support from Laserlab-Europe (LENS002289, Grant No. 654148) and the Royal Netherlands Academy of Arts and Sciences (KNAW). The Swiss Study Foundation is acknowledged for a fellowship to M.M.L. We thank P. van der Meulen for support with the temperature dependent NMR *in situ*-irradiation studies and T. Tiemersma-Wegman for ESI-MS analyses.

REFERENCES

(1) Brieke, C.; Rohrbach, F.; Gottschalk, A.; Mayer, G.; Heckel, A. Light-Controlled Tools. *Angew. Chem., Int. Ed.* **2012**, *51* (34), 8446−8476.

(2) Ankenbruck, N.; Courtney, T.; Naro, Y.; Deiters, A. Optochemical Control of Biological Processes in Cells and Animals. *Angew. Chem., Int. Ed.* **2018**, *57* (11), 2768−2798.

(3) *Molecular Switches*, 2nd ed.; Feringa, B. L., Browne, W. R., Eds.; Wiley-VCH: Weinheim, Germany, 2011.

(4) Bouas-Laurent, H.; Dürr, H. Organic Photochromism (IUPAC Technical Report). *Pure Appl. Chem.* **2001**, *73* (4), 639−665.

(5) Alfimov, M. V.; Fedorova, O. A.; Gromov, S. P. Photoswitchable Molecular Receptors. *J. Photochem. Photobiol., A* **2003**, *158* (2−3), 183−198.

(6) Iwaso, K.; Takashima, Y.; Harada, A. Fast Response Dry-Type Artificial Molecular Muscles with [C2]Daisy Chains. *Nat. Chem.* **2016**, *8* (6), 625−632.

(7) Balzani, V.; Credi, A.; Raymo, F. M.; Stoddart, J. F. Artificial Molecular Machines. *Angew. Chem., Int. Ed.* **2000**, *39* (19), 3348−3391.

(8) Kay, E. R.; Leigh, D. A. Rise of the Molecular Machines. *Angew. Chem., Int. Ed.* **2015**, *54* (35), 10080−10088.

(9) Erbas-Cakmak, S.; Leigh, D. A.; McTernan, C. T.; Nussbaumer, A. L. Artificial Molecular Machines. *Chem. Rev.* **2015**, *115* (18), 10081−10206.

(10) Russew, M.-M.; Hecht, S. Photoswitches: From Molecules to Materials. *Adv. Mater.* **2010**, *22* (31), 3348−3360.

(11) Wang, L.; Li, Q. Photochromism into Nanosystems: Towards Lighting up the Future Nanoworld. *Chem. Soc. Rev.* **2018**, *47* (3), 1044−1097.

(12) Beharry, A. A.; Woolley, G. A. Azobenzene Photoswitches for Biomolecules. *Chem. Soc. Rev.* **2011**, *40* (8), 4422−4437.

(13) Szymański, W.; Beierle, J. M.; Kistemaker, H. A. V.; Velema, W. A.; Feringa, B. L. Reversible Photocontrol of Biological Systems by the Incorporation of Molecular Photoswitches. *Chem. Rev.* **2013**, *113* (8), 6114−6178.

(14) Velema, W. A.; Szymański, W.; Feringa, B. L. Photopharmacology: Beyond Proof of Principle. *J. Am. Chem. Soc.* **2014**, *136* (6), 2178−2191.

(15) Broichhagen, J.; Frank, J. A.; Trauner, D. A Roadmap to Success in Photopharmacology. *Acc. Chem. Res.* **2015**, *48* (7), 1947−1960.

(16) Lerch, M. M.; Hansen, M. J.; van Dam, G. M.; Szymanski, W.; Feringa, B. L. Emerging Targets in Photopharmacology. *Angew. Chem., Int. Ed.* **2016**, *55* (37), 10978−10999.

(17) Hüll, K.; Morstein, J.; Trauner, D. In Vivo Photopharmacology. *Chem. Rev.* **2018**, *118* (21), 10710−10747.

(18) Tochitsky, I.; Kienzler, M. A.; Isacoff, E.; Kramer, R. H. Restoring Vision to the Blind with Chemical Photoswitches. *Chem. Rev.* **2018**, *118* (21), 10748−10773.

(19) Bandara, H. M. D.; Burdette, S. C. Photoisomerization in Different Classes of Azobenzene. *Chem. Soc. Rev.* **2012**, *41* (5), 1809−1825.

(20) Wiedbrauk, S.; Dube, H. Hemithioindigo - An Emerging Photoswitch. *Tetrahedron Lett.* **2015**, *56* (29), 4266−4274.

(21) Irie, M.; Yokoyama, Y. Diarylethenes for Memories and Switches. *Chem. Rev.* **2000**, *100* (5), 1685−1716.

(22) Helmy, S.; Leibfarth, F. A.; Oh, S.; Poelma, J. E.; Hawker, C. J.; Read de Alaniz, J. Photoswitching Using Visible Light: A New Class of Organic Photochromic Molecules. *J. Am. Chem. Soc.* **2014**, *136* (23), 8169−8172.

(23) Helmy, S.; Oh, S.; Leibfarth, F. A.; Hawker, C. J.; Read de Alaniz, J. Design and Synthesis of Donor-Acceptor Stenhouse Adducts: A Visible Light Photoswitch Derived from Furfural. *J. Org. Chem.* **2014**, *79* (23), 11316−11329.

DOI: 10.1021/jacs.9b00341
J. Am. Chem. Soc. 2019, 141, 7376−7384

(24) Hemmer, J. R.; Poelma, S. O.; Treat, N.; Page, Z. A.; Dolinski, N. D.; Diaz, Y. J.; Tomlinson, W.; Clark, K. D.; Hooper, J. P.; Hawker, C. J.; Read De Alaniz, J. Tunable Visible and Near Infrared Photoswitches. *J. Am. Chem. Soc.* **2016**, *138* (42), 13960−13966.
(25) Mallo, N.; Brown, P. T.; Iranmanesh, H.; MacDonald, T. S. C.; Teusner, M. J.; Harper, J. B.; Ball, G. E.; Beves, J. E. Photochromic Switching Behaviour of Donor-acceptor Stenhouse Adducts in Organic Solvents. *Chem. Commun.* **2016**, *52* (93), 13576−13579.
(26) Hemmer, J. R.; Page, Z. A.; Clark, K. D.; Stricker, F.; Dolinski, N. D.; Hawker, C. J.; Read de Alaniz, J. Controlling Dark Equilibria and Enhancing Donor-Acceptor Stenhouse Adduct Photoswitching Properties through Carbon Acid Design. *J. Am. Chem. Soc.* **2018**, *140* (33), 10425−10429.
(27) Lerch, M. M.; Szymański, W.; Feringa, B. L. The (Photo)-Chemistry of Stenhouse Photoswitches: Guiding Principles and System Design. *Chem. Soc. Rev.* **2018**, *47* (6), 1910−1937.
(28) Barachevsky, V. A. Negative Photochromism in Organic Systems. *Rev. J. Chem.* **2017**, *7* (3), 334−371.
(29) Lerch, M. M.; Wezenberg, S. J.; Szymański, W.; Feringa, B. L. Unraveling the Photoswitching Mechanism in Donor-Acceptor Stenhouse Adducts. *J. Am. Chem. Soc.* **2016**, *138* (20), 6344−6347.
(30) Di Donato, M.; Lerch, M. M.; Lapini, A.; Laurent, A. D.; Iagatti, A.; Bussotti, L.; Ihrig, S. P.; Medved', M.; Jacquemin, D.; Szymański, W.; Buma, W. J.; Foggi, P.; Feringa, B. L. Shedding Light on the Photoisomerization Pathway of Donor-Acceptor Stenhouse Adducts. *J. Am. Chem. Soc.* **2017**, *139* (44), 15596−15599.
(31) Lerch, M. M.; Medved', M.; Lapini, A.; Laurent, A. D.; Iagatti, A.; Bussotti, L.; Szymański, W.; Buma, W. J.; Foggi, P.; Di Donato, M.; Feringa, B. L. Tailoring Photoisomerization Pathways in Donor-Acceptor Stenhouse Adducts: The Role of the Hydroxy Group. *J. Phys. Chem. A* **2018**, *122* (4), 955−964.
(32) Bull, J. N.; Carrascosa, E.; Mallo, N.; Scholz, M. S.; da Silva, G.; Beves, J. E.; Bieske, E. J. Photoswitching an Isolated Donor-Acceptor Stenhouse Adduct. *J. Phys. Chem. Lett.* **2018**, *9* (3), 665−671.
(33) Lerch, M. M.; Di Donato, M.; Laurent, A. D.; Medved', M.; Iagatti, A.; Bussotti, L.; Lapini, A.; Buma, W. J.; Foggi, P.; Szymański, W.; Feringa, B. L. Solvent Effects on the Actinic Step of Donor-Acceptor Stenhouse Adduct Photoswitching. *Angew. Chem., Int. Ed.* **2018**, *57* (27), 8063−8068.
(34) Nieto Faza, O.; Silva López, C.; Álvarez, R.; de Lera, Á. R. Theoretical Study of the Electrocyclic Ring Closure of Hydroxypentadienyl Cations. *Chem. - Eur. J.* **2004**, *10* (17), 4324−4333.
(35) Piutti, C.; Quartieri, F. The Piancatelli Rearrangement: New Applications for an Intriguing Reaction. *Molecules* **2013**, *18* (10), 12290−12312.
(36) Riveira, M. J.; Marsili, L. A.; Mischne, M. P. The Iso-Nazarov Reaction. *Org. Biomol. Chem.* **2017**, *15* (44), 9255−9274.
(37) Griffiths, P. R.; Foskett, C. T.; Curbelo, R. Rapid Scan Infrared Fourier Transform Spectroscopy. *Appl. Spectrosc. Rev.* **1972**, *6* (1), 31−77.
(38) Becke, A. D. Density-Functional Thermochemistry. III. The Role of Exact Exchange. *J. Chem. Phys.* **1993**, *98* (7), 5648−5652.
(39) Stephens, P. J.; Devlin, F. J.; Chabalowski, C. F.; Frisch, M. J. Ab Initio Calculation of Vibrational Absorption and Circular Dichroism Spectra Using Density Functional Force Fields. *J. Phys. Chem.* **1994**, *98* (45), 11623−11627.
(40) Papajak, E.; Zheng, J.; Xu, X.; Leverentz, H. R.; Truhlar, D. G. Perspectives on Basis Sets Beautiful: Seasonal Plantings of Diffuse Basis Functions. *J. Chem. Theory Comput.* **2011**, *7* (10), 3027−3034.
(41) Marenich, A. V.; Cramer, C. J.; Truhlar, D. G. Universal Solvation Model Based on Solute Electron Density and on a Continuum Model of the Solvent Defined by the Bulk Dielectric Constant and Atomic Surface Tensions. *J. Phys. Chem. B* **2009**, *113* (18), 6378−6396.
(42) Zhao, Y.; Truhlar, D. G. The M06 Suite of Density Functionals for Main Group Thermochemistry, Thermochemical Kinetics, Noncovalent Interactions, Excited States, and Transition Elements: Two New Functionals and Systematic Testing of Four M06-Class Functionals and 12 Other Function. *Theor. Chem. Acc.* **2008**, *120* (1−3), 215−241.
(43) Johnson, E. R.; Mori-Sánchez, P.; Cohen, A. J.; Yang, W. Delocalization Errors in Density Functionals and Implications for Main-Group Thermochemistry. *J. Chem. Phys.* **2008**, *129* (20), 204112.
(44) Snellenburg, J. J.; Laptenok, S. P.; Seger, R.; Mullen, K. M.; van Stokkum, I. H. M. Glotaran: A Java -Based Graphical User Interface for the R Package TIMP. *J. Stat. Softw.* **2012**, *49* (3), 1−22.
(45) Mallo, N.; Foley, E. D.; Iranmanesh, H.; Kennedy, A. D. W.; Luis, E. T.; Ho, J.; Harper, J. B.; Beves, J. E. Structure-Function Relationships of Donor-Acceptor Stenhouse Adduct Photochromic Switches. *Chem. Sci.* **2018**, *9* (43), 8242−8252.
(46) In SI section 4, we report for completeness fs UV/vis transient absorption studies on DASA **1** in DCM that have not been reported in our previous work.[30,33]

DOI: 10.1021/jacs.9b00341
J. Am. Chem. Soc. 2019, 141, 7376−7384